



**HAL**  
open science

## Mechanical properties of pyrolysed wood – a nanoindentation study

Gerald Zickler, Thomas Schöberl, Oskar Paris

► **To cite this version:**

Gerald Zickler, Thomas Schöberl, Oskar Paris. Mechanical properties of pyrolysed wood – a nanoindentation study. *Philosophical Magazine*, 2006, 86 (10), pp.1373-1386. 10.1080/14786430500431390 . hal-00513635

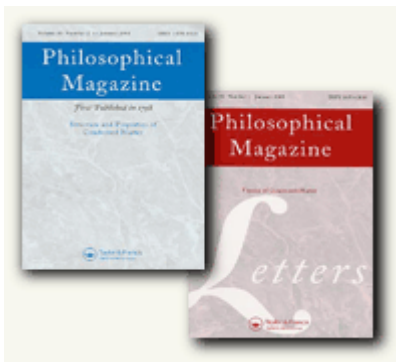
**HAL Id: hal-00513635**

**<https://hal.science/hal-00513635>**

Submitted on 1 Sep 2010

**HAL** is a multi-disciplinary open access archive for the deposit and dissemination of scientific research documents, whether they are published or not. The documents may come from teaching and research institutions in France or abroad, or from public or private research centers.

L'archive ouverte pluridisciplinaire **HAL**, est destinée au dépôt et à la diffusion de documents scientifiques de niveau recherche, publiés ou non, émanant des établissements d'enseignement et de recherche français ou étrangers, des laboratoires publics ou privés.



**Mechanical properties of pyrolysed wood – a nanoindentation study**

Journal:	<i>Philosophical Magazine &amp; Philosophical Magazine Letters</i>
Manuscript ID:	TPHM-05-Apr-0091.R1
Journal Selection:	Philosophical Magazine
Date Submitted by the Author:	22-Sep-2005
Complete List of Authors:	Zickler, Gerald; Max Planck Institute KGF, Biomaterials; Max Planck Institute of Colloids and Interfaces, Biomaterials Schöberl, Thomas; Austrian Academy of Sciences, Erich Schmid Institute of Materials Science Paris, Oskar; Max Planck Institute of Colloids and Interfaces, Biomaterials; Max Planck Institute KGF, Biomaterials
Keywords:	nanoindentation, mechanical properties, carbon
Keywords (user supplied):	wood, pyrolysis



## Mechanical properties of pyrolysed wood – a nanoindentation study

G. A. ZICKLER<sup>†</sup>, T. SCHÖBERL<sup>‡</sup> and O. PARIS<sup>†\*</sup>

<sup>†</sup>Max Planck Institute of Colloids and Interfaces, Department of Biomaterials, Am Mühlenberg 1,  
D-14476 Potsdam-Golm, Germany

<sup>‡</sup>Erich Schmid Institute of Materials Science, Austrian Academy of Sciences and Institute of Metal  
Physics, University of Leoben, Jahnstr. 12, A-8700 Leoben, Austria

\*Corresponding author: e-Mail: [oskar.paris@mpikg.mpg.de](mailto:oskar.paris@mpikg.mpg.de) (O. Paris)

The present work is focused on changes of mechanical properties in pyrolysed spruce wood as a function of temperature up to 2400°C. Nanoindentation tests are used for the determination of mechanical properties at the scale of single wood cell walls. Hardness, indentation modulus and elasto-plastic/brittle behaviour of the carbonaceous residues are derived as function of pyrolysis temperature. Hardness values increase continuously by more than one order of magnitude to 4.5 GPa at 700°C. The indentation modulus shows complex changes with a minimum of 5 GPa around 400°C and a maximum of 40 GPa around 1000°C. The deformation induced by the indenter is largely visco-plastic in native wood, but it is almost purely elastic in the carbonaceous residue with particular low values of the indentation ductility index around 700°C. A low density and a strongly cross-linked carbon structure may explain the mechanical behaviour at these intermediate temperatures. A final decrease of the modulus and a slight decrease of ductility for temperatures above 2000°C can be attributed to a continuous structural transition of the material towards graphite-like stacking of carbon sheets and to preferred carbon orientation along the wood cell axis.

*Keywords:* Wood; Carbon; Pyrolysis; Nanoindentation; Mechanical properties

## 1. Introduction

Natural plant resources present a large potential for transforming hierarchically ordered and mechanically optimised structures into carbonaceous materials by simple pyrolysis processes. They have been used for millennia to generate charcoal [1], and also for quite some years to produce activated carbons with high micro- and mesoporosity for filters or catalyst supports [2-4]. These applications do not usually require preservation of the hierarchical structure, and the mechanical integrity of the precursor is not retained. However, there is a growing interest of a one-to-one transformation of the unique anatomical characteristics of plants into structural materials with entirely different composition, overcoming eventually some physical limitations of the biological precursor.

Carbonised wood monoliths can be used as templates for near net shape manufacturing of a diversity of materials, including structural activated carbons, carbon/polymer- and carbon/carbon composites as well as carbide- or oxide ceramics [5-12]. In particular the cellular morphology of wood tissues and the large diversity of their pore sizes and size distributions promise a broad range of potential applications such as filters, catalyst carriers, biocatalysts, sensors or even cancellous bone replacement [9]. Consequently, a growing number of current research activities is concentrating on structural aspects of wood pyrolysis [13-17], in particular concerning fundamental questions of the carbon nanostructure development and preferred carbon orientation as a possible consequence of the cellulose microfibril orientation in wood [13; 17].

Concerning its mechanical properties, wood is a material of excellent optimisation strategies at several levels of hierarchy. Apart from macroscopic optimisation [18] a cellular honeycomb-like structure at the micrometre level provides high directional stiffness and strength at low weight [19]. Another optimisation is performed at the nanometre level where the so-called cellulose microfibril angle controls the needs either for high stiffness or for high extensibility of the cell walls, and this provides an adaptive tool for the tree to react upon external stresses [20-22]. Moreover, subtle deformation mechanisms at the molecular scale allow large plastic deformation of the cell wall material without damage [23]. Upon pyrolytic conversion some of these optimisation features might be transferred into the inorganic carbonaceous material by retaining preferred orientation as well as the nanocomposite character. Thus, some of the architectural optimisations in wood may be combined with the superior properties of composite carbon materials such as high tensile modulus and tensile strength at very high temperatures. However, there are only a few investigations of the mechanical properties of pyrolysed wood [7; 8; 14; 24; 25], and to the best of our knowledge, there are no studies of the mechanical properties on the level of single cell walls.

1  
2  
3  
4  
5  
6  
7  
8  
9  
10  
11  
12  
13  
14  
15  
16  
17  
18  
19  
20  
21  
22  
23  
24  
25  
26  
27  
28  
29  
30  
31  
32  
33  
34  
35  
36  
37  
38  
39  
40  
41  
42  
43  
44  
45  
46  
47  
48  
49  
50  
51  
52  
53  
54  
55  
56  
57  
58  
59  
60

Nanoindentation provides the ability to measure both elastic and plastic deformation at a very small scale [26; 27]. Thus, it can be used for the characterisation of hardness and elastic modulus, as well as other elastic and plastic parameters of the carbonaceous residue after wood pyrolysis at the level of single cell walls. The method was applied to study native wood by Wimmer *et al.* [28; 29], and it was shown that it can provide new insights into local mechanical properties of the wood cell wall. Gindl *et al.* extended this matter, investigating the influence of lignin content [30], microfibril angle [31] and chemical wood modifications [32; 33] on local mechanical properties. A critical discussion about the general significance of mechanical parameters from nanoindentation tests on wood samples was provided by Gindl and Schöberl [34], regarding the effect of high elastic anisotropy on the indentation modulus. The present work is focusing on changes of mechanical properties of cell walls from spruce wood by pyrolysis up to temperatures of 2400°C with narrow temperature intervals. Additionally to the mechanical parameters, mass loss and dimensional changes of the material are determined as a function of heat treatment temperature, from which the bulk density change of the material is obtained. The aim of this work is to continuously follow the development of the mechanical response of the material during decomposition of wood and the subsequent formation of carbon. Together with the structural changes published elsewhere [17], we derive a detailed survey of the relation between local microstructures and mechanical properties of biomorphous carbon from wood.

## 2. Experimental Methods

A board of air dried spruce wood (*Picea abies* Karst.) of error-free quality with year rings of regular intervals containing normal wood with small microfibril angle was selected for the experiment. The samples were stored in an environmental chamber, kept at 20°C and a relative ambient moisture content of 65% before machining. Cubic shaped specimens of 15×15×15 mm<sup>3</sup> size were cut using a band saw in a way that the faces of the cubes were parallel to the axial, radial and tangential growth directions of the tree. Prior and after pyrolysis the specimens were weighed and axial, radial and tangential dimensions were measured using a micrometre screw. Macroscopic bulk density was calculated by taking the sample mass and dividing it by the volume determined from macroscopic dimensions. Five samples were heat treated at every temperature value between 220°C and 600°C with intervals of 20°C and between 600°C and 1000°C with intervals of 100°C. This was performed in a tube furnace (Heraeus Thermicon) equipped with a quartz glass tube under continuous flow of nitrogen gas (approximately 0.02 m<sup>3</sup> h<sup>-1</sup>) to ensure a non-oxidising atmosphere. For all specimens the heating rate was 2°C min<sup>-1</sup>. Further specimens were pyrolysed at 1300°C, 1600°C, 2200°C and 2400°C after pre-pyrolysis at 1000°C in a vacuum-seal inert gas furnace (HTM Reetz) under

1  
2 continuous argon flow with a heating rate of  $5^{\circ}\text{C min}^{-1}$ . The maximum temperature was maintained  
3  
4 for 2 h before cooling to room temperature. Thereafter shrinkage data and mass loss of the samples  
5  
6 were determined, and then they were stored in an environmental chamber under conditions  
7  
8 described above. Inspections of the pyrolysed samples with light microscopy and scanning electron  
9  
10 microscopy (SEM) revealed that the original cellular structure of wood was retained without visible  
11  
12 signs of macroscopic cracks or other defects introduced by the pyrolytic treatment.

13 In order to study the mechanical properties with nanoindentation, the wood specimens were  
14  
15 embedded into PMMA. SEM was used to show that the lumens of the wood cells were not filled  
16  
17 with the embedding media, and therefore a potential influence could be excluded.

18 The surface perpendicular to the axial direction was grinded and polished to characterise the  
19  
20 mechanical behaviour of the tracheid cell wall. Then the samples were glued on metal plates and  
21  
22 magnetically clamped on the motorized XYZ staging system of the indentation device. Mechanical  
23  
24 tests were done with a Hysitron Ubi1<sup>®</sup> nanoindenter (Hysitron Inc., Minneapolis, MN, USA), which  
25  
26 was mounted on a vibration isolation platform to minimise the influence of environmental  
27  
28 vibrations. The testing machine was placed in an acoustic enclosure, which had been designed to  
29  
30 lessen the amount of acoustic noise, block air currents and act as a thermal buffer to eliminate drifts.  
31  
32 An optical microscope with a CCD detector attached to the nanoindentation device was used to  
33  
34 examine the sample surface. In a subsequent step, areas of  $50 \times 50 \mu\text{m}^2$  in latewood regions were  
35  
36 scanned with the indenter tip, where spots in the middle of latewood cell walls were selected for  
37  
38 indentation testing. Only latewood cells with a thickness of several  $\mu\text{m}$  were used, in order to  
39  
40 minimise possible artefacts from cell wall borders.

41 The nanoindentation system monitored the penetration depth and the indentation load  
42  
43 continuously during the loading and unloading segments of the indentation procedure. All load-  
44  
45 displacement data were obtained with a three sided diamond pyramid (Berkovich-type) [27; 29].  
46  
47 For the indentation tests a loading/unloading procedure according to suitable, recently developed,  
48  
49 optimisation criteria was used [29; 31; 33; 34]. Every experiment consisted of six segments (see  
50  
51 figure 1a). [Insert figure 1 about here.] The indenter tip was loaded in a force-controlled mode to a  
52  
53 peak force of  $250 \mu\text{N}$  at a rate of  $50 \mu\text{N s}^{-1}$ . The following hold segment of 30 s at constant load  
54  
55 was used to monitor visco-plastic creep. In the unloading segment the force was programmed to  
56  
57 decrease to 20% of the maximum, where a second hold segment of 15 s was used to estimate visco-  
58  
59 elastic recovery, before the sample was completely unloaded. An average number of 25 indents on  
60  
radial and tangential latewood cell walls of different wood year rings were performed on every  
specimen. The obtained load-displacement curves were corrected for thermal drift and for machine  
compliance. Figure 1b shows a nanoindentation curve of spruce wood pyrolysed at  $220^{\circ}\text{C}$ , and the  
viscous behaviour can clearly be seen.

The key parameters obtained during indentation experiments were peak load  $P_{\max}$ , the displacement at peak load  $h$  and the unloading stiffness  $S$ . According to the method developed by Oliver and Pharr [27], based on considerations by Doerner and Nix [26], the elastic modulus of a sample, which exhibits plastic deformation during loading, was determined from the initial unloading curve, which was supposed to be purely elastic. The analysis of the load-displacement curves proceeded with the determination of the reduced elastic modulus  $E_r$  from the slope  $S$  of a tangent to the initial unloading curve segment, where  $A$  is the projected area of contact between the investigated material and the indenter at maximum load:

$$E_r = \frac{\sqrt{\pi}}{2} \frac{S}{\sqrt{A}} \quad (1)$$

From the known geometry of the indenter body (Berkovich-type pyramid [27; 29]) and the indentation depth  $h$ , the contact area was calculated. The reduced modulus  $E_r$  accounts for the effect of elastic deformation of the indenter based on the assumption that compliance occurs in the indenter as well as in the sample. The definition of  $E_r$  adapted from Stillwell and Tabor [35] is therefore:

$$\frac{1}{E_r} = \frac{1-\nu^2}{E} + \frac{1-\nu_i^2}{E_i} \quad (2)$$

$E$  and  $\nu$  are the elastic modulus and Poisson's ratio of the sample, and  $E_i$  and  $\nu_i$  are the same parameters of the indenter tip. It has to be pointed out that for rather soft materials like wood  $E$  and  $E_r$  are almost identical. Hardness  $H$  is defined by  $H = P_{\max} / A$ .

The concept of energy-based considerations on the elastic-plastic deformation by pyramidal type indenters was described by Sakai [36]. The total work done by the indenter to cause elastic and plastic deformation, when the indenter reaches the maximum depth and the work done by the solid to the indenter during unloading, have been examined, and an indentation ductility index  $D$  was defined by [37]:

$$D = \frac{U_r}{U_t} \quad (3)$$

The hysteresis loop energy is named  $U_r$ . The total energy  $U_t$ , which is needed to create an indentation impression at  $P_{\max}$ , is the sum of  $U_r$  and the elastic stored energy  $U_e$ , which is released during unloading. According to this definition, the indentation ductility index  $D$  is equal to one for a fully plastic material without any elastic recovery during unloading, and it is equal to zero for a fully elastic material exhibiting a complete unloading recovery in an elastic manner along its previous loading path.

### 3. Results

### 3.1. Bulk density change

The strongest dimensional changes of spruce wood are observed in a narrow interval between 220°C to 320°C. With further increasing heat treatment temperature, shrinkage proceeds at a lower rate, ceasing at about 800°C for the axial direction, and going through a slight maximum for the radial and tangential direction at about 1500°C. These results are in accordance with earlier investigations [13]. Generally the reduction in length is strongly anisotropic, being about 24% in the axial direction, about 38 % in radial and about 42% in tangential direction at 2400°C. Similar to the dimensional changes, the major mass loss (approximately 60%) of the specimens occurs predominantly within the small temperature interval between 220°C and 320°C. At temperatures above 420°C only very small relative mass changes are observed, reaching a final carbon yield of about 20 wt% at 2400°C. Clear shoulders in the mass loss as well as in the volumetric shrinkage data at 280°C and 340°C demonstrate the major decomposition of hemicelluloses and cellulose, respectively, in good accordance with earlier investigations [6; 13; 24]. Figure 2 shows the effect of pyrolysis temperature on the macroscopic density change  $\rho/\rho_0$  of spruce wood, derived from the mass- and volume changes. [Insert figure 2 about here.]  $\rho$  is the actual density at temperature  $T$ , and  $\rho_0$  is the density of the native wood at room temperature ( $\rho_0 = 0.49 \text{ g cm}^{-3}$ ). At temperatures up to about 340°C the loss of volatile matter predominates and results in an overall decrease of the macroscopic density to about 60% of the original wood density. Apparently, no significant density changes occur in the temperature range between 340°C and 600°C, which means that the apparent mass loss is accompanied by a corresponding volume change. Above 600°C, the density increases and displays a relative maximum at about 900°C and a minimum at about 1800°C, reaching eventually a value of 80% of the original wood density at 2400°C.

### 3.2. Nanoindentation

Load-displacement curves from nanoindentation experiments on pyrolysed spruce cell walls clearly display the elastic and plastic changes of the material after different heat treatments. For better illustration figure 3 is split into two parts with different scales on the horizontal axis. [Insert figure 3 about here.] Figure 3a shows selected load-displacement curves (averages of 25 indentation experiments on different cell walls) on samples pyrolysed at temperatures from 220°C to 1000°C, and figure 3b covers the temperature range from 1300°C to 2400°C. It can be seen that the slope of the unloading curve changes with increasing pyrolysis temperature up to 1000°C. A decrease of the maximum displacement of the material is observed. The hysteresis between the loading and

1  
2 unloading curves represents the energy dissipated by the indentation. The sample pyrolysed at  
3 220°C shows typical elasto-plastic behaviour with an obvious hysteresis loop enclosed by the paths  
4 of loading and unloading, and a large residual indent remains at the surface after complete  
5 unloading. In contrast, the load-displacement curve of the specimen pyrolysed at 1000°C, the  
6 unloading curve follows closely the loading path back to the origin of the curve with no significant  
7 amount of energy dissipation and without any residual indent. With increasing pyrolysis  
8 temperatures up to about 1000°C the indentation response changes gradually from elasto-plastic to  
9 brittle, almost purely elastic behaviour. Interestingly, in the temperature range from 1300°C to  
10 2400°C (see figure 3b) this material response is reversed. The slope of the unloading segment  
11 clearly decreases from 1300°C to 2200°C and 2400°C, while the hysteresis loop broadens again.

12  
13 The quantitative analysis of the nanoindentation tests reveals an average reduced elastic  
14 modulus  $E_r$  of  $14.19 \pm 1.56$  GPa, a hardness  $H$  of  $0.40 \pm 0.04$  GPa and a ductility index  $D$  of  $0.75 \pm$   
15  $0.03$  for native untreated secondary cell walls of spruce wood. These values are in good agreement  
16 with previously published works on mechanical properties of the wood cell wall [20; 29-34]. The  
17 effects of pyrolysis temperature on the mechanical properties of wood cell walls are shown in  
18 figures 4, 5 and 6 (mean values over 25 measurements, error bars denote standard deviations).  
19 Figure 4 shows the effect of pyrolysis temperature on  $E_r$ . Up to a temperature of about 280°C only a  
20 slight decrease of  $E_r$  is observed, whereas the curve drops very fast to about half of the original  
21 value between 280°C and 320°C and displays a characteristic broad minimum around 400°C.  
22 [Insert figure 4 about here.] Starting at about 500°C,  $E_r$  rises up by almost an order of magnitude to  
23 approximately 40 GPa at 900°C and stays then constant at this value until 1600°C. At 2200°C and  
24 2400°C a significant decline of  $E_r$  can be observed. In figure 5 the hardness shows a continuous  
25 increase from around 0.4 GPa at 220°C to approximately 4.5 GPa at 700°C, remaining  
26 approximately constant at this maximum, until a reversal of the trend is observed again at  
27 temperatures above 2000°C [Insert figure 5 about here.]. Figure 6 illustrates the effect of the heat  
28 treatment temperature on the indentation ductility index  $D$ , which stays almost constant at  $D \approx 0.8$   
29 up to temperatures of 300°C and then decreases rapidly to a value below  $D \approx 0.1$ . A clear minimum  
30 of  $D \approx 0.03$  at about 700°C corresponds to the temperature, where also the maximum hardness  
31 value is reached [Insert figure 6 about here.]. Local maxima at 500°C, from 1000°C to 1200°C and  
32 at 2400°C indicate a very high sensitivity of this energy based parameter to subtle structural and/or  
33 compositional changes with temperature.

#### 4. Discussion

1  
2 The effects of pyrolysis temperature on mechanical properties of the cell wall material from wooden  
3 precursor can roughly be separated into three temperature regions: i)  $T < 400^{\circ}\text{C}$ , ii)  $T = 400^{\circ}\text{C}$  to  
4  $1000^{\circ}\text{C}$  and iii)  $T > 1000^{\circ}\text{C}$ . The choice of these intervals is based on apparent changes in the  
5 mechanical parameters derived from nanoindentation of the cell wall material (see figures 4-6), and  
6 corresponds also to characteristic turnover regions in the bulk density (see figure 2). Moreover,  
7 these regions coincide roughly with temperature intervals identified in a previous work on structural  
8 changes during wood pyrolysis [17], indicating a close correlation between the changes of density,  
9 nanostructural parameters and mechanical properties. A particularly interesting temperature regime  
10 is found between  $700^{\circ}\text{C}$  and  $900^{\circ}\text{C}$ , showing maximum values of the reduced elastic modulus,  
11 hardness and apparent density and a minimum of plastic deformability.  
12  
13

14  
15  
16  
17  
18  
19  
20 When discussing the changes of mechanical properties of the cell wall material upon  
21 pyrolysis, one should correct the measured mechanical parameters for porosity. In the present work  
22 the bulk density is determined, which includes the contributions from macroporosity (i.e., the cell  
23 lumens) as well as from meso- and microporosity of the cell wall material. On the other hand, the  
24 mechanical parameters have been measured at the cell wall level, and they are only influenced by  
25 meso- and microporosity. As long as water content and chemical composition change strongly  
26 during pyrolysis ( $200^{\circ}\text{C}$  to  $600^{\circ}\text{C}$ ), the bulk density changes are rather difficult to be related to  
27 porosity. If it is assumed that the material maintains its structural integrity (no cracks or  
28 delaminations), and no surface evaporation leads to preferential cell wall thinning, the  
29 macroporosity at the cellular level remains roughly constant. Thus, for temperatures above  $600^{\circ}\text{C}$ ,  
30 the bulk density changes in figure 2 can approximately be related to the cell wall level, being  
31 induced by microporosity development and by material densification. Comparing the absolute  
32 changes in figures 4 and 5 with those in figure 2, it is obvious that porosity changes are in the order  
33 of 30% to 40% above  $600^{\circ}\text{C}$ , while the values for modulus and hardness change by almost one  
34 order of magnitude. Thus, porosity development will influence the mechanical parameters only  
35 slightly concerning their absolute values, but not concerning the general trends, which will be  
36 discussed in the following.  
37  
38  
39  
40  
41  
42  
43  
44  
45  
46  
47  
48  
49

50 In region i), the changes of elastic modulus  $E_r$  of spruce wood cell walls as function of  
51 pyrolysis temperature (see figure 4) appears to be controlled by the combined effects of chemical  
52 and physical changes [17]. For temperatures below  $250^{\circ}\text{C}$  only evaporation of water and  
53 dehydration together with slight depolymerisation were observed, and no significant structural  
54 changes regarding crystallinity, shape, size and orientation of cellulose microfibrils were found. In  
55 the temperature region from  $250^{\circ}\text{C}$  to  $350^{\circ}\text{C}$ , X-ray scattering investigations identified the complete  
56 degeneration of cellulose microfibrils, resulting in an apparent disintegration of the whole  
57 microstructure with neither orientational nor positional correlations at the nanometre level. The  
58  
59  
60

1  
2 mechanical parameters derived in the present work - in particular the elastic modulus - render this  
3 trend perfectly in the corresponding temperature region. Up to 250°C there are almost no changes in  
4 the mechanical properties. The rapid decrease of  $E_r$  with increasing pyrolysis temperature between  
5 250°C and 350°C is clearly associated with the degradation of the biopolymers, in particular with  
6 cellulose which is known to provide stiffness to the wood material. Evaporation of low molecular-  
7 weight volatile matter, substantial chemical changes and a decrease in apparent density (see figure  
8 2) all contribute in a complex manner to the drop of  $E_r$  and to the changes in hardness and plastic  
9 response. It is interesting to note that the minimum of the elastic modulus between 350°C and  
10 450°C corresponds to a minimum of density (see figure 2) and to a fully disintegrated structure  
11 [17], best described by a highly defective, open structure of molecular fragments (tars, chars), with  
12 pores of less than 0.5 nm in size resulting from the release of gaseous decomposition products.

13  
14  
15  
16  
17  
18  
19  
20  
21 In region ii),  $E_r$  and  $H$  increase while the indentation ductility index  $D$  decreases strongly,  
22 indicating the transition from a ductile polymeric biomaterial to a brittle, glass-like material.  
23 Compression tests on macroscopic pyrolysed wood samples showed similar effects of heat  
24 treatment temperature on mechanical properties, where the compressive strength first decreased to a  
25 minimum and then increased again above 500°C to 600°C [8; 25]. Kercher and Nagle [14]  
26 performed a series of four-point bending tests of carbonised medium-density fibreboards. The  
27 authors considered these materials as isotropic and calculated a Young's modulus of the bulk  
28 material under the assumption of an open-cell foam model. Data in the temperature range from  
29 600°C to 1000°C were presented and the elastic modulus displays a fairly linear increase from  
30 about 20 GPa to 40 GPa. In the present study  $E_r$  rises from approximately 17 GPa to 38 GPa in this  
31 temperature range, which is in excellent agreement with the previous investigation. Interestingly,  
32 also the bulk density increases from 600°C to 900°C, with a distinct maximum at 900°C. A similar  
33 densification trend in this temperature regime was already reported by Byrne and Nagle [13] and  
34 others [2], who attributed this fact to the closing of micropores.

35  
36  
37  
38  
39  
40  
41  
42  
43  
44  
45  
46 For pyrolysis temperatures above 1000°C (region iii)), it seems reasonable to compare the  
47 results of the present investigation with indentation tests on various bulk carbon materials, as for  
48 example glassy carbon [38-44], pyrolytic graphite, coke [39], and carbon-carbon composites [45-  
49 47]. In figure 3b the slope of the load-displacement curves decreases with increasing heat treatment  
50 temperature, and the unloading path does not completely retrace the loading path but fairly well  
51 returns to the origin of the curve with a small hysteretic loop. Indentation studies on glassy carbon  
52 materials and heat-treated carbons reported similar behaviour in the temperature range from about  
53 1000°C to 3000°C [38; 41; 42; 44]. The maximum indentation depths of these materials  
54 progressively increased, indicating easier penetration and "softening" of the material, and the  
55 hysteresis loop of the indentation process in the loading-unloading cycle was also enlarged with  
56  
57  
58  
59  
60

1  
2 increasing temperature. The elastic modulus of glassy carbon measured with conical micro-  
3 indenters was found to reduce from 31 GPa to 21 GPa [41], and hardness decreased from 6.9 GPa to  
4 3.7 GPa [42] in the range from 1000°C to 3000°C. Rodrigues *et al.* [43] investigated polymeric  
5 glassy carbon materials from 300°C to 2500°C, and they measured a maximum hardness value of  
6 about 2.5 GPa at 1000°C. It can thus be concluded that the absolute values of the high temperature  
7 mechanical properties for pyrolysed wood are quite comparable to glassy carbon materials.  
8 Moreover, the maximum of hardness and elastic modulus at around 1000°C with a subsequent  
9 considerable decrease seems to be a general finding for disordered carbonaceous materials.  
10

11  
12 Structurally, the pyrolysed wood material appears fully amorphous at 350°C, followed by  
13 successive ordering at the molecular scale (aromatisation) and at the nanometre scale (density  
14 fluctuations and/or micropore growth) [17]. The continuous increase of  $E_r$  in the temperature range  
15 of 500°C to 900°C displays this carbonisation process characterised by increasing covalent carbon  
16 bonding. Interestingly, the hardness reaches a maximum value already at a considerably lower  
17 temperature than the elastic modulus (at about 700°C) while the indentation ductility index  $D$   
18 approaches a clear minimum value close to zero at this temperature. A low-density, glass-like 3D  
19 network consisting of a high amount of cross-linking between adjacent (aromatic) carbon sheets  
20 could be responsible for such behaviour. Taking the elemental analysis on cellulose by Tang and  
21 Bacon [48; 49] as representative also for wood, less than 5 at% of oxygen, but around 20 at% of  
22 hydrogen can be expected in the carbonaceous residue above 600°C. Such a high H-content could  
23 enable a significant amount of  $sp^3$ -type bonding, similarly to a class of materials known as a-C:H,  
24 or diamond-like carbons [50]. But also for pure carbon, covalent  $sp^3$ -type cross-linking between  
25 graphene sheets of  $sp^2$  bonded carbon has just recently been reported. On the basis of *ab-initio*  
26 calculations, Telling *et al.* [51] showed that certain point defect configurations such as di-vacancies  
27 can lead to covalent bridges between adjacent graphene layers in graphite. Similar types of cross-  
28 links were recently identified in carbon nanotube bundles to be responsible for an enormous  
29 increase of the bending modulus induced by electron irradiation [52]. Since the carbonaceous  
30 residue from pyrolysed wood contains presumably a high concentrations of vacancy-like defects  
31 from the evaporation of volatile molecular fragments, such energetically metastable cross-links  
32 could contribute significantly to the carbon structure at low temperatures. Thus, the structure of  
33 pyrolysed wood between 600°C and 1000°C might be rather similar to amorphous, strongly 3D-  
34 crosslinked carbon, quite different to turbostratic, graphite-like carbon. Such a structure can  
35 qualitatively explain the high hardness and the extremely low indentation ductility index. Heat  
36 treatments at higher temperatures (region iii)) partially eliminate these cross-links and successively  
37 transform the low-density, rigid carbon-networks into turbostratic stacks of carbon sheets, with  
38 increasing graphite-like character [15]. The reduction of elastic modulus and hardness with the  
39  
40  
41  
42  
43  
44  
45  
46  
47  
48  
49  
50  
51  
52  
53  
54  
55  
56  
57  
58  
59  
60

1  
2 increase of heat treatment temperature above 2000°C could be additionally coupled to the  
3 development of preferred carbon orientation. A growing degree of preferred orientation of graphene  
4 sheets in pyrolysed wood was indeed found for higher temperatures [17], which could relieve  
5 slipping mechanisms of turbostratic carbon sheets, thus reducing the hardness. Moreover, increasing  
6 graphitisation leads to a decrease of the elastic constants  $C_{33}$  and  $C_{44}$ , while  $C_{11}$  strongly increases.  
7 Since all these elastic constants influence the indentation modulus in a complex manner in an  
8 orientated material, the decrease of  $E_r$  with temperature could well be an orientation effect, similar  
9 to the case of oriented cellulose in native wood [34]. However, preferred orientation alone cannot  
10 provide a satisfactory explanation, since glassy carbon materials with no preferred orientation show  
11 a quite similar qualitative and quantitative behaviour [41; 42; 44]. Moreover, also porosity cannot  
12 be made responsible for the effect, since the material density increases above 2000°C (i.e. decrease  
13 of porosity), which should result in an increase of  $E$ . Based on these considerations it is proposed,  
14 that the unexpected mechanical properties of pyrolysed wood around 1000°C are a consequence of  
15 a particular structure, based on a low-density 3D carbon network with a high amount of cross-  
16 linking. This structure is thought to be quite different from the turbostratic carbon found at higher  
17 temperatures, which is based on stacks of  $sp^2$ -bonded graphene sheets, allowing sliding of the basal  
18 panes and therefore an increasing ability to deform plastically. Mechanical deformation of this very  
19 hard and brittle material at intermediate temperatures is only possible via the creation of cracks,  
20 which partially close upon unloading, giving an almost perfect elastic response of the material.  
21 Compared to other indentation studies of bulk carbon materials, the peak loads in the present study  
22 are very low, and the load-displacement curves give no hint of a significant discontinuity in the  
23 loading curve, as observed by other authors [40; 42; 47]. Therefore, there is no direct evidence for  
24 formation and growth of macrocrack systems and immersions in the stress field under the indenter  
25 tip, but of course a development of microscopic cracks cannot be disclaimed.

26  
27  
28  
29  
30  
31  
32  
33  
34  
35  
36  
37  
38  
39  
40  
41  
42  
43  
44 Finally, we note an interesting observation concerning the ratio of hardness to elastic  
45 modulus  $H/E_r$ , which is of significant interest in both, fracture mechanics and tribology. Cheng and  
46 Cheng [53] investigated the relationship between this ratio and the indentation ductility index  $D$ .  
47 Remarkably, an almost linear relationship was found within the range of  $D$  from 0.2 to 1.0, based  
48 on a large number of finite element calculations. Good agreement was found with experimental data  
49 from several metals and ceramics, covering a large range of  $D$ . Figure 7 shows that this linear  
50 correlation between  $H/E_r$  and  $D$  holds also fairly well for pyrolysed spruce wood as long as  $D$  is  
51 larger than about 0.1. However, at smaller values of  $D$  this relationship breaks down, indicating  
52 again a fundamentally different deformation mechanism of the carbonaceous residue in the region  
53 around 1000°C, where  $D$  is considerably smaller than 0.1. [Insert figure 7 about here.]  
54  
55  
56  
57  
58  
59  
60

## 5. Conclusion

Mechanical properties of the carbon materials from pyrolysed wood have been measured at the cell wall level over a wide temperature range. Elastic modulus, hardness and elastic/plastic behaviour show distinct changes with temperature. Below 400°C decomposition of the wood biopolymers (in particular cellulose) leads to a minimum of the elastic modulus. Above 400°C a continuous increase of elastic modulus, hardness and a gradual transition from a visco-plastic biomaterial into a brittle, glass-like carbonaceous residue is observed. At around 800°C elastic modulus and hardness reach maximum values which are about one order of magnitude larger than the minimum values. At the same temperatures the plastic deformation described by the indentation ductility index  $D$  has almost vanished, and the material behaves purely elastic. At temperatures above 2000°C elastic modulus and hardness decrease markedly, while the plastic deformability of the material clearly improves. The peculiar mechanical behaviour at intermediate temperatures around 1000°C is attributed qualitatively to a particular nanostructure of the carbonaceous material, consisting of a strongly cross-linked 3D carbon network, quite different from the graphite-like, turbostratic stacking of extended carbon sheets present at higher temperatures. Mechanical deformation of this material under the indenter is thought to be solely controlled by the formation and growth of microcracks which close again upon unloading. A fundamentally different deformation mechanism within this intermediate temperature regime is also supported by finite element calculations from literature. While the ratio  $H/E_r$  follows closely the predicted behaviour for values of the indentation ductility index  $D$  above 0.1 (corresponding to low and high pyrolysis temperatures), this is not the case for the intermediate temperatures, where  $D$  is very low.

## Acknowledgement

The authors would like to thank I. Burgert from Max Planck Institute of Colloids and Interfaces, Department of Biomaterials (Potsdam, Germany) for providing the wood specimens and for valuable discussions on the topic, and C. Zollfrank from the Department of Materials Science, Friedrich-Alexander University of Erlangen-Nürnberg (Erlangen, Germany) for his aid with the heat treatments. We are thankful to E. Haberz and G. Moser from the Erich Schmid Institute, and the Metal Physics Institute, University of Leoben (Leoben, Austria) for patient and assiduous sample preparation. Financial support from the Max Planck Society is gratefully acknowledged.

## References

1  
2  
3  
4  
5  
6  
7  
8  
9  
10  
11  
12  
13  
14  
15  
16  
17  
18  
19  
20  
21  
22  
23  
24  
25  
26  
27  
28  
29  
30  
31  
32  
33  
34  
35  
36  
37  
38  
39  
40  
41  
42  
43  
44  
45  
46  
47  
48  
49  
50  
51  
52  
53  
54  
55  
56  
57  
58  
59  
60

- [1] M. J. Antal and M. Grønli, *Ind. Eng. Chem. Res.* **42** 1619 (2003).
- [2] E. R. Buiel, A. E. George and J. R. Dahn, *Carbon* **37** 1399 (1999).
- [3] A. K. Kercher and D. C. Nagle, *Carbon* **41** 3 (2003).
- [4] R. Asakura, M. Morita, K. Maruyama, H. Hatori and Y. Yamada, *J. Mater. Sci.* **39** 201 (2004).
- [5] C. E. Byrne and D. C. Nagle, *Mat. Res. Inovat.* **1** 137 (1997).
- [6] P. Greil, T. Lifka and A. Kaindl, *J. Eur. Ceram. Soc.* **18** 1961 (1998).
- [7] P. Greil, T. Lifka and A. Kaindl, *J. Eur. Ceram. Soc.* **18** 1975 (1998).
- [8] H. Iizuka, M. Fushitani, T. Okabe and K. Saito, *J. Porous Mater.* **6** 175 (1999).
- [9] P. Greil, *J. Eur. Ceram. Soc.* **21** 105 (2001).
- [10] E. Vogli, H. Sieber and P. Greil, *J. Eur. Ceram. Soc.* **22** 2663 (2002).
- [11] C. Zollfrank, R. Kladny, H. Sieber and P. Greil, *J. Eur. Ceram. Soc.* **24** 479 (2004).
- [12] C. Zollfrank and H. Sieber, *J. Eur. Ceram. Soc.* **24** 495 (2004).
- [13] C. E. Byrne and D. C. Nagle, *Carbon* **35** 267 (1997).
- [14] A. K. Kercher and D. C. Nagle, *Carbon* **40** 1321 (2002).
- [15] A. K. Kercher and D. C. Nagle, *Carbon* **41** 15 (2003).
- [16] C. Zollfrank and O. Paris, in *Proc. 12<sup>th</sup> Int. Symp. Wood & Pulping Chem.*, (University of Wisconsin-Madison, Madison, Wisconsin) 349 (2003).
- [17] O. Paris, C. Zollfrank and G. A. Zickler, *Carbon* **43** 53 (2005).
- [18] C. Mattheck and H. Kubler, *Wood: The Internal Optimization of Trees* (Springer, Berlin, 1995).
- [19] L. J. Gibson, M. F. Ashby, G. N. Karam, U. Wegst and H. R. Shercliff, *Proc. R. Soc. Lond. A* **450** 141 (1995).
- [20] A. Reiterer, H. Lichtenegger, S. Tschegg and P. Fratzl, *Phil. Mag. A* **79** 2173 (1999).
- [21] H. Lichtenegger, A. Reiterer, S. E. Stanzl-Tschegg and P. Fratzl, *J. Struct. Biology* **128** 257 (1999).
- [22] J. Färber, H. C. Lichtenegger, A. Reiterer, S. Stanzl-Tschegg and P. Fratzl, *J. Mater. Sci.* **36** 5087 (2001).
- [23] J. Keckes, I. Burgert, K. Frühmann, M. Müller, K. Kölln, M. Hamilton, M. Burghammer, S. V. Roth, S. Stanzl-Tschegg and P. Fratzl, *Nature Materials* **2** 810 (2003).
- [24] C. E. Byrne and D. C. Nagle, *Carbon* **35** 259 (1997).
- [25] M. Kumar, B. B. Verma and R. C. Gupta, *Energy Sources* **21** 675 (1999).
- [26] M. F. Doerner and W. D. Nix, *J. Mater. Res.* **1** 601 (1986).
- [27] W. C. Oliver and G. M. Pharr, *J. Mater. Res.* **7** 1564 (1992).
- [28] R. Wimmer and B. N. Lucas, *IAWA J.* **18** 77 (1997).
- [29] R. Wimmer, B. N. Lucas, T. Y. Tsui and W. C. Oliver, *Wood Sci. Technol.* **31** 131 (1997).

- 1  
2 [30] W. Gindl, H. S. Gupta and C. Grünwald, *Can. J. Bot.* **80** 1029 (2002).  
3  
4 [31] W. Gindl, H. S. Gupta, T. Schöberl, H. C. Lichtenegger and P. Fratzl, *Appl. Phys. A* **79** 2069  
5 (2004).  
6  
7 [32] W. Gindl and H. S. Gupta, *Composites A* **33** 1141 (2002).  
8  
9 [33] W. Gindl, T. Schöberl and G. Jeronimidis, *Int. J. Adhes. Adhes.* **24** 279 (2004).  
10  
11 [34] W. Gindl and T. Schöberl, *Composites A* **35** 1345 (2004).  
12  
13 [35] N. A. Stillwell and D. Tabor, *Proc. Phys. Soc.* **78** 169 (1961).  
14  
15 [36] M. Sakai, *Acta metall. mater.* **41** 1751 (1993).  
16  
17 [37] M. Sakai, *J. Mater. Res.* **14** 3650 (1999).  
18  
19 [38] M. Sakai, H. Hanyu and M. Inagaki, *J. Am. Ceram. Soc.* **78** 1006 (1995).  
20  
21 [39] J. S. Field and M. V. Swain, *Carbon* **34** 1357 (1996).  
22  
23 [40] M. V. Swain and J. S. Field, *Phil. Mag. A* **74** 1085 (1996).  
24  
25 [41] N. Iwashita, M. V. Swain, J. S. Field, N. Ohta and S. Bitoh, *Carbon* **39** 1525 (2001).  
26  
27 [42] N. Iwashita, J. S. Field and M. V. Swain, *Phil. Mag. A* **82** 1873 (2002).  
28  
29 [43] M. G. Rodrigues, N. C. da Cruz, E. C. Rangel, R. L. Zimmerman, D. Ila, D. B. Poker and D. K.  
30 Hensley, *Nucl. Instrum. Methods Phys. Res. B* **191** 524 (2002).  
31  
32 [44] M. Sakai, Y. Nakano and S. Shimizu, *J. Am. Ceram. Soc.* **85** 1522 (2002).  
33  
34 [45] M. Kanari, K. Tanaka, S. Baba and M. Eto, *Carbon* **35** 10 (1997).  
35  
36 [46] D. T. Marx and L. Riester, *Carbon* **37** 1679 (1999).  
37  
38 [47] P. Diss, J. Lamon, L. Carpentier, J. L. Loubet and P. Kapsa, *Carbon* **40** 2567 (2002).  
39  
40 [48] M. M. Tang and R. Bacon, *Carbon* **2** 211 (1964).  
41  
42 [49] R. Bacon and M. M. Tang, *Carbon* **2** 221 (1964).  
43  
44 [50] J. Robertson, *Mater. Sci. Eng. R.* **37** 129 (2002).  
45  
46 [51] R. H. Telling, C. P. Ewels, A. A. El-Barbary, M. I. Heggie, *Nature Materials* **2** 333 (2003).  
47  
48 [52] A. Kis, G. Csanyi, J. P. Salvétat, T. N. Lee, E. Coureau, A. J. Kulik, W. Benoit, J. Brugger, L.  
49 Forro, *Nature Materials* **3** 152 (2004).  
50  
51 [53] Y.-T. Cheng and C.-M. Cheng, *Appl. Phys. Lett.* **73** 614 (1998).  
52  
53  
54  
55  
56  
57  
58  
59  
60

1  
2  
3  
4  
5  
6  
7  
8  
9  
10  
11  
12  
13  
14  
15  
16  
17  
18  
19  
20  
21  
22  
23  
24  
25  
26  
27  
28  
29  
30  
31  
32  
33  
34  
35  
36  
37  
38  
39  
40  
41  
42  
43  
44  
45  
46  
47  
48  
49  
50  
51  
52  
53  
54  
55  
56  
57  
58  
59  
60

## Figure Captions

**Figure 1:** (a) Loading procedure (load versus time) for nanoindentation tests on pyrolysed wood cell walls. Every indentation test consisted of six segments: (1) loading, (2) holding, (3) unloading, (4) holding and (5) total unloading. (b) Typical load-displacement curve of spruce wood heat treated at 220°C showing the segments denoted above.

**Figure 2:** Effect of pyrolysis temperature on the macroscopic density changes of spruce wood char.

**Figure 3:** A series of averaged load-displacement curves from nanoindentation experiments illustrating the elastic and plastic behaviour of spruce wood cell walls pyrolysed at different temperatures (a) 220°C to 1000°C and (b) 1300°C to 2400°C. Individual temperatures are indicated in the figures.

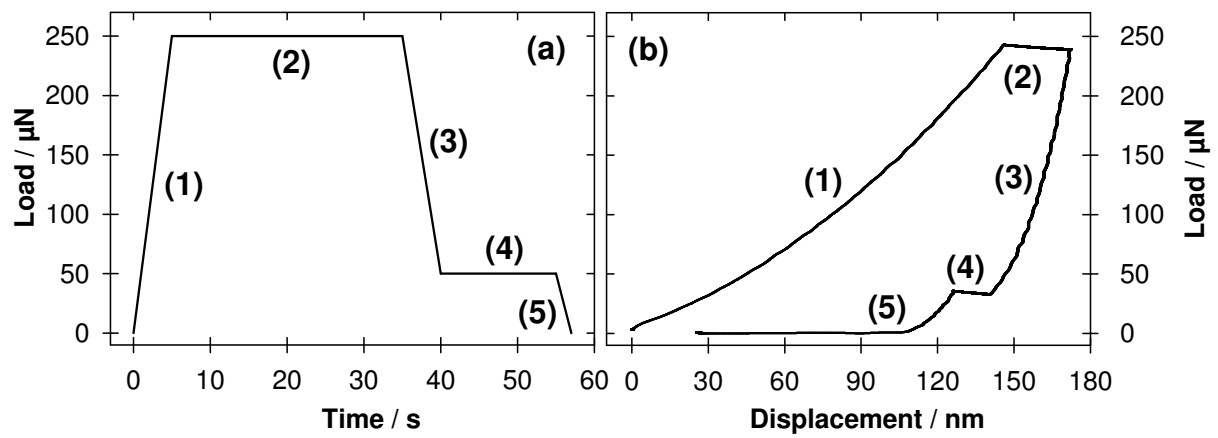
**Figure 4:** Reduced elastic modulus  $E_r$  of pyrolysed spruce wood cell wall material as function of heat treatment temperature.

**Figure 5:** Hardness of pyrolysed spruce wood cell wall material as function of heat treatment temperature.

**Figure 6:** Indentation ductility index of pyrolysed spruce wood cell wall material as function of heat treatment temperature.

**Figure 7:** Relationship between the ratio of hardness to reduced elastic modulus  $H/E_r$  and the indentation ductility index  $D$  of spruce wood cell wall material pyrolysed at different temperatures. The dashed line indicates the numerical results by Cheng and Cheng [53].

Figure 1: Zickler et al.



1  
2  
3  
4  
5  
6  
7  
8  
9  
10  
11  
12  
13  
14  
15  
16  
17  
18  
19  
20  
21  
22  
23  
24  
25  
26  
27  
28  
29  
30  
31  
32  
33  
34  
35  
36  
37  
38  
39  
40  
41  
42  
43  
44  
45  
46  
47  
48  
49  
50  
51  
52  
53  
54  
55  
56  
57  
58  
59  
60

Figure 2: Zickler et al.

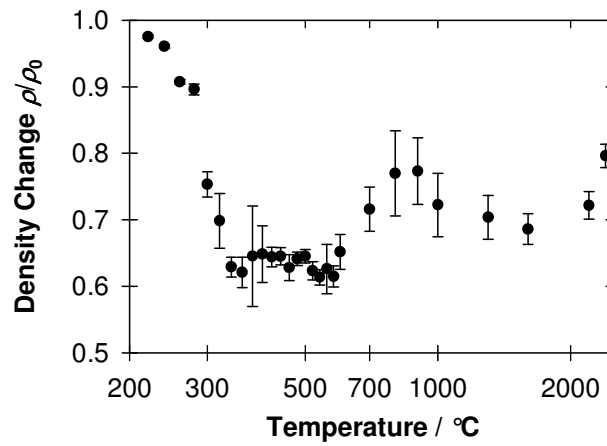
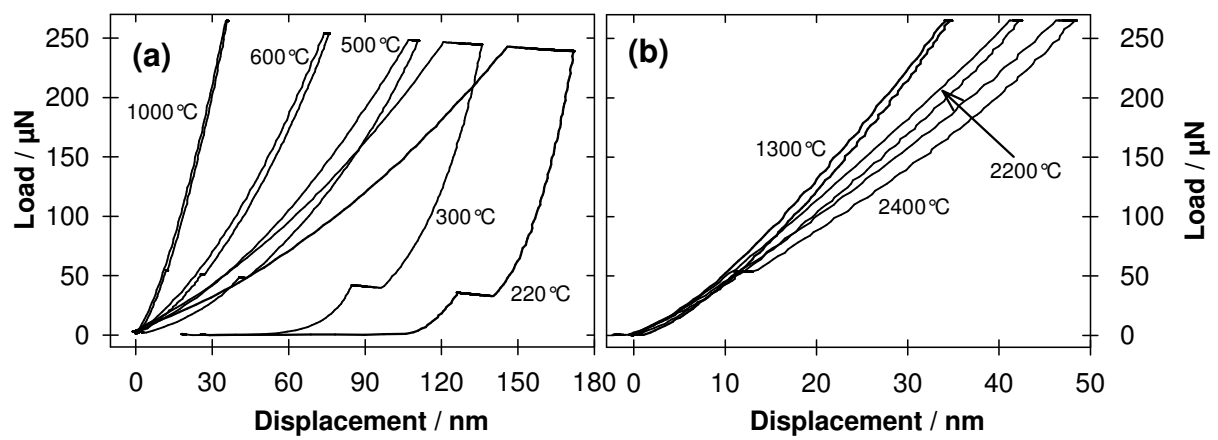


Figure 3: Zickler et al.



1  
2  
3  
4  
5  
6  
7  
8  
9  
10  
11  
12  
13  
14  
15  
16  
17  
18  
19  
20  
21  
22  
23  
24  
25  
26  
27  
28  
29  
30  
31  
32  
33  
34  
35  
36  
37  
38  
39  
40  
41  
42  
43  
44  
45  
46  
47  
48  
49  
50  
51  
52  
53  
54  
55  
56  
57  
58  
59  
60

Figure 4: Zickler et al.

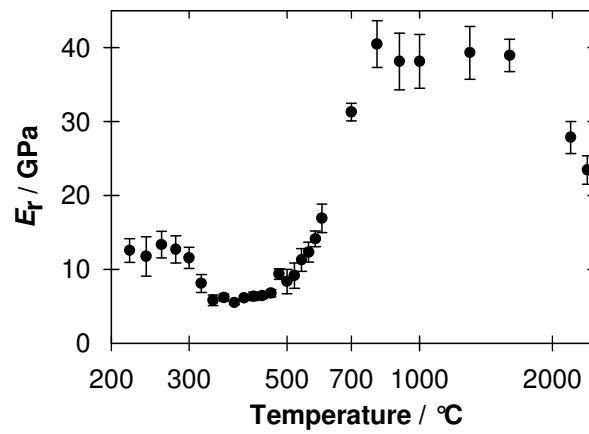


Figure 5: Zickler et al.

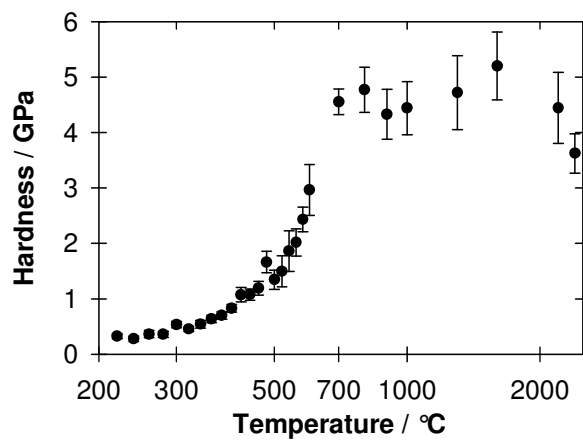


Figure 6: Zickler *et al.*

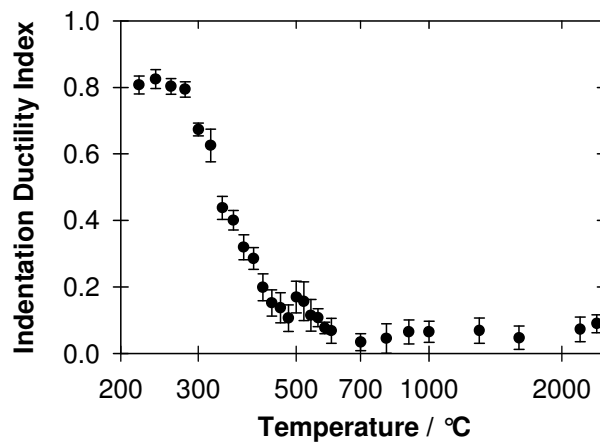




Figure 1: Zickler et al.

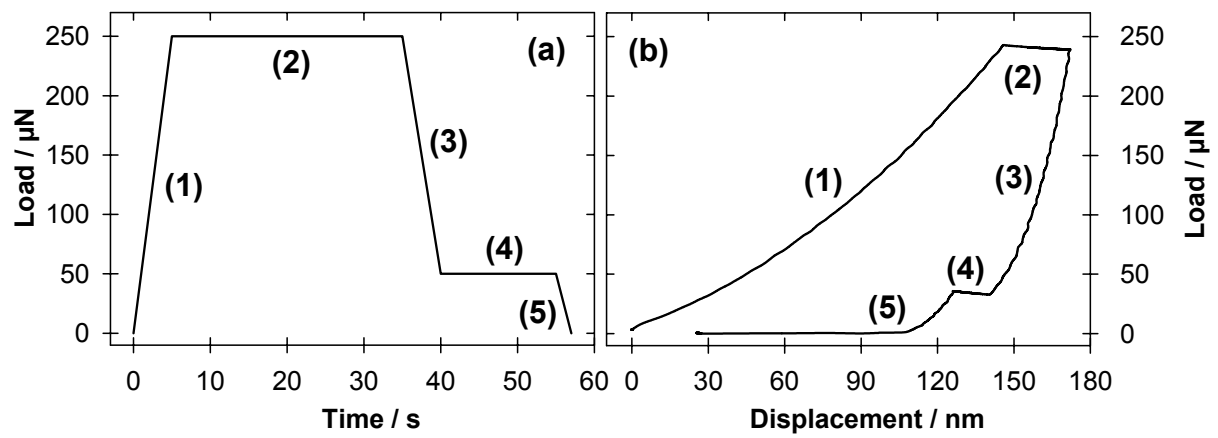


Figure 2: Zickler *et al.*

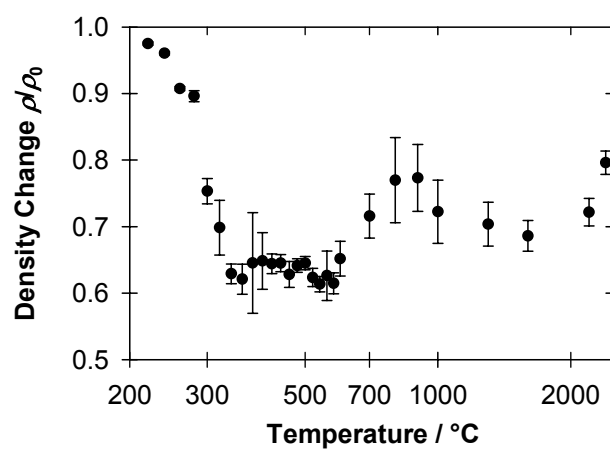


Figure 3: Zickler et al.

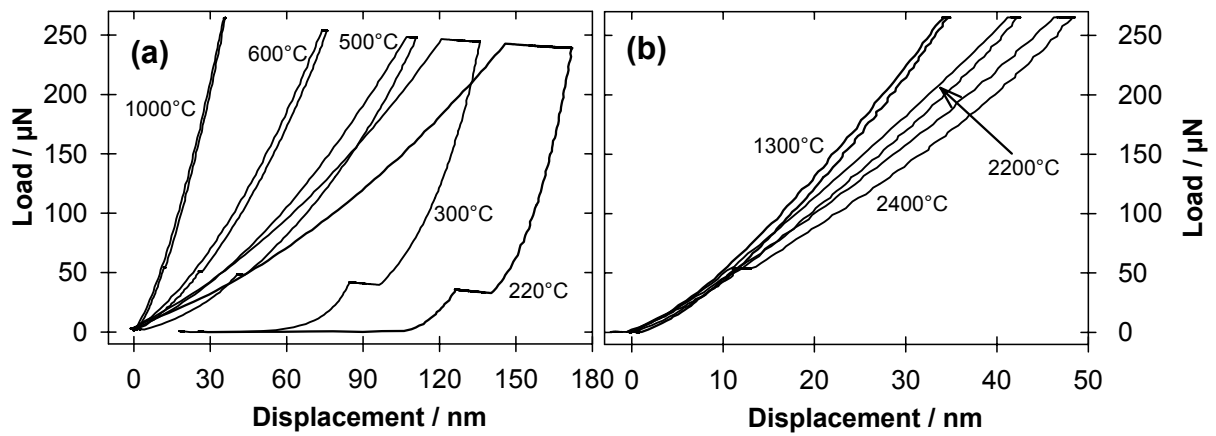
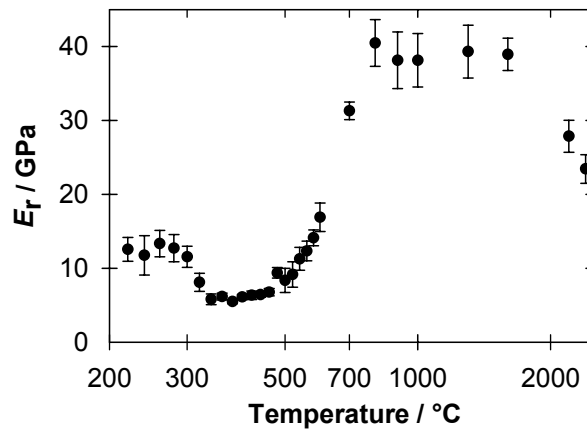


Figure 4: Zickler *et al.*



1  
2  
3  
4  
5  
6  
7  
8  
9  
10  
11  
12  
13  
14  
15  
16  
17  
18  
19  
20  
21  
22  
23  
24  
25  
26  
27  
28  
29  
30  
31  
32  
33  
34  
35  
36  
37  
38  
39  
40  
41  
42  
43  
44  
45  
46  
47  
48  
49  
50  
51  
52  
53  
54  
55  
56  
57  
58  
59  
60

Figure 5: Zickler et al.

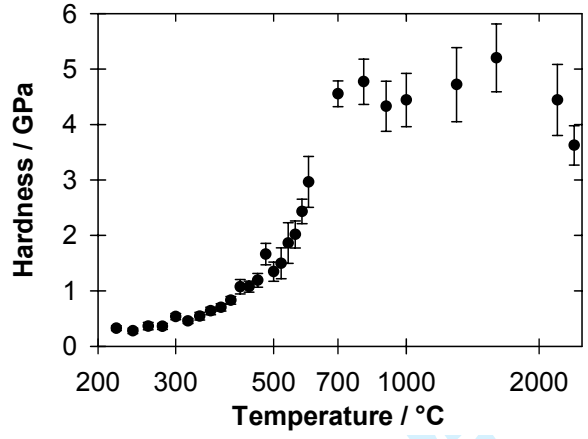


Figure 6: Zickler *et al.*

